Study on Cell Deformation of Low Porosity Aluminum Foams under Quasi-Static Compression by X-Ray Tomography

Ningzhen Wang, Xiang Chen, Éric Maire, Paul H. Kamm, Ying Cheng, Yanxiang Li, Francisco Garcia-Moreno

ADVANCED ENGINEERING MATERIALS
www.aem-journal.com

Study on Cell Deformation of Low Porosity Aluminum Foams under Quasi-Static Compression by X-Ray Tomography

*Ningzhen Wang, Xiang Chen, Eric Maire, Paul H. Kamm, Ying Cheng, Yanxiang Li, and Francisco García-Moreno**

Understanding the correlation between cell deformation and initial cell structure during compression is important for improvement and development of effective applications of aluminum foams. Foams with porosities lower than 75% now get more attention because of more spherical cells and better mechanical performance. Herein, two low porosity aluminum foam samples are deformed by a compressive device allowing simultaneous X-ray tomography. The foam cell structures in the initial undeformed state and in the state, where the first batch of cells deforms, are characterized and correlated. The absolute value of anisotropy change is selected as the most sensitive parameter to evaluate the cell deformation. A fitting formula between the cell deformation degree and the initial cell parameters is obtained, which can predict the cell deformation degree. It is found that a cell with small anisotropy, large angle between the longest axis of the cell and the loading direction, small sphericity, more neighbors, and large cell size is more prone to deform during compression. With the fitting formula, the weakest region where the first batch of deformed cells occurs can be predicted. The influence of cell morphology parameters in low porosity aluminum foams is significant and verified by experimental results.

1. Introduction

Closed-cell aluminum foams have been widely used in automotive, ship building, railway, aerospace, building decoration, and other fields.[1,2] In addition to functionalities, such as noise reduction, fire retardance, and electromagnetic shielding, properties, such as lightweight and high-energy absorption, are the main advantages of aluminum foams.[2] The mechanical properties of aluminum foams are related to their relative densities, cell structures, and base alloys.[3–7] Regardless of base alloys, the counterpart of the mechanical properties at cell level is the cell deformation. X-ray tomography makes it possible to obtain the 3D cell structure of aluminum foam non-destructively.[8,9] If the cell deformation and failure can be predicted by the initial cell structure, an optimized direction of foam structure could be provided for preparation, and then, the mechanical properties could be improved.[10–12] Moreover, the first failure region of an aluminum foam piece could be known in advance[13] and prevented through reinforcement, which is significant for applications.

Usually, there is a stress plateau stage in the typical compression stress–strain curve of an aluminum foam.[3] Cells gradually undergo plastic deformation and collapse during this stage, where most of the energy is absorbed.[14,15] The status after the elastic deformation and just entering the stress plateau stage is what we concerned. Hangai et al.[13] predicted the first deformation layer according to the maximum stress region in the finite-element (FE) simulation. Digital image correlation (DIC) is a powerful tool to measure the strain evolution of specimen surface.[16,17] Sun et al.[18] used DIC to obtain the strain concentration region in the 2D meso-scale structure of closed-cell aluminum foam and found that the first crush band and weakest region can be determined by the minimum ratio of cell wall thickness and cell wall length. However, the structure is equivalent to a 3D tubular structure

Dr. N. Wang, Dr. F. García-Moreno
Materials Science and Technology
Technische Universität Berlin
Hardenbergstraße 36, 10623 Berlin, Germany
E-mail: garcia-moreno@helmholtz-berlin.de

The ORCID identification number(s) for the author(s) of this article can be found under https://doi.org/10.1002/adem.202000264.

DOI: 10.1002/adem.202000264

Dr. N. Wang, Dr. X. Chen, Dr. Y. Cheng, Prof. Y. Li
School of Materials Science and Engineering
Tsinghua University
100084 Beijing, China

Dr. E. Maire
MATEIS, CNRS UMR5510
INSA de Lyon
Université de Lyon
69621 Villeurbanne, France

Dr. P. H. Kamm, Dr. F. García-Moreno
Institute of Applied Materials
Helmholtz-Zentrum Berlin für Materialien und Energie
Hahn-Meitner-Platz 1, 14109 Berlin, Germany

with the corresponding cellular cross section, which is different from a 3D closed cell structure. In situ X-ray tomography has been developed rapidly these years for studying the evolution of 3D structures of cellular materials during compression.[19–23] Kader et al.[20] correlated the geometrical and topological characteristics with the deforming microstructure of high porosity aluminum foams (>80%) under dynamic loading. Digital volume correlation (DVC) can be used to characterize the interior strain concentration based on the tomography results.[24,25] Jiroušek et al.[25] tracked the deforming evolution of aluminum foam at low strain conditions using DVC algorithm. Assisted with in situ X-ray tomography and DVC, Chai et al.[21,22] determined the spatial distribution of the weakest cell walls by an edge segmentation method and strength index of cell walls, and porosities of the studied PMI foams were both larger than 90%. The 3D deformation of low porosity PDMS foam (40–60%) during compression was also studied, but the morphology influence of individual cells was not clarified.[19] The 3D cell deformation of low porosity aluminum foams (<75%) has not been reported to the best of our knowledge.

Regardless of the role of entrapped gas in closed cells under impact condition,[26] the strength of aluminum foam is mainly contributed by the solid skeleton.[27,28] Therefore, many previous experimental and numerical studies on the deformation of aluminum foams were based on the failure modes of solid part or cell walls.[29–32] To improve the mechanical properties, aluminum foams with small and fine cells were fabricated by increasing foaming pressure or improving blowing agent in Alporas route, which correspondingly reduces the porosity.[33–35] Aluminum foams with low porosity and uniform cells usually have spherical cells and thick cell walls.[36,37] Spherical cells make it difficult to extract the cell wall flakes from 3D structure through, e.g., the method of edge segmentation.[21,22] For thick cell walls, it is not easy to find plastic hinges that cause buckling in the first deformation stage.[37] Therefore, a research method based on deformation evolution of cell walls is not suitable for aluminum foams with low porosity (<75%). The deformation of solid parts or cell walls indirectly causes the change of the cell structure, and changing cell parameters, such as coordination number, anisotropy, sphericity, and cell orientation, also reflects changing of cell walls. The compressive test equipment assisted with X-ray tomography allows for obtaining the 3D cell morphology of aluminum foams during the deformation process.[14,23] Therefore, changes of each single 3D cell structure are used to characterize the deformation of aluminum foams in this article. Every cell could be tracked until the first batch of cell deforms, and the changes of cell parameters can be obtained and correlated with the initial cell parameters.

Parameters that affect the cell deformation are listed according to previous studies: 1) Local density. Studies by Meguid et al.,[38] Hangai et al.,[39] and Zhang et al.[15] all indicated that it has an influence on deformation localization of aluminum foam, and the deformation starts from the low-density region. 2) Anisotropy. The anisotropy of a sphere is defined as 0 and the flattest shape as 1 in the following for convenience. Influences of cell anisotropy on cell deformation are not consistent in previous research. FE simulation by Kadkhodapour and Raeisi[5] showed that a foam with elliptic cells has higher plateau stress than a foam with round cells; namely, the cell with larger anisotropy is more difficult to deform. Saadatfar et al.[40] also suggested that the region with small cell anisotropy is more likely to induce deformation bands. However, other research[6] showed that a large cell anisotropy of cells reduced the mechanical properties of aluminum foam. 3) Sphericity. Yang et al.[41] found that non-spherical cells reduce the effective elastic modulus of aluminum foams compared with spherical cells. 4) Direction of the longest axis of cells. Many studies[6,42] have shown that loading along the longest axis of cells yields higher mechanical response of aluminum foams. 5) Cell size. It has been studied that the aluminum foam with small cell sizes has better mechanical properties than with large cell sizes even at the same density.[4,15] 6) Cell wall thickness. Research of Kader et al.[32] showed that cells with a thicker cell wall were compressed less.

In this article, two aluminum foam samples produced following the Alporas method were compressed under quasi-static condition, and the process was interrupted by applying X-ray tomography for studying the evolution of foam deformation. Cells of each foam at the initial undeformed state and at the state when the first batch of cells deforms were both characterized and tracked. The correlation between the deformation degree and the initial cell parameters was built. The effects of initial cell parameters on cell deformation were quantitatively analyzed. The first deformation region with severely deformed cells could be predicted. Influence of cell morphology on cell deformation was verified by the experimental results.

2. Experimental Section

2.1. Sample Preparation

The two aluminum foam samples tested in this article were both prepared by the Alporas method. During the preparation, Ca was added into pure aluminum melt for thickening, followed by TiH_2 as blowing agent. That way, a solid aluminum foam block could be obtained after the foaming and solidification processes.[36]

It has been already studied that a high relative density is conducive to high mechanical properties of aluminum foams.[3] Usually, reducing cell size helps to increase relative density of the foam and improve the stability of cells.[37,43] To reduce the cell size, pre-oxidized TiH_2 powder was mixed with Cu powder by ball milling, and the mixed powders were used as blowing agent. The detailed preparation process is described in the literature.[34] Limited by the size of the compressive device, the dimensions of the two samples were around 8 mm × 8 mm × 10 mm. A tomographic slice of each sample is shown in **Figure 1**a,b, and cells are quite spherical. Overall porosities of foams #1 and #2 are 62.0% and 73.3%, respectively. Figure 1c exhibits the porosity distributions of tomography slices along the three directions, and the thickness of one slice is 8 μm. It could be seen that the two samples are relatively uniform, and there is no serious low-density region around the samples. As cell size and coordination number of a cell could reflect the local density to some extent, cell parameters should be the main factors, affecting the initial deformation of foams. It was suggested that the size effect in compressive test could be avoided when the ratio of specimen size to cell size is at least larger than 6.[44,45] In addition, there are few structural defects in the two samples

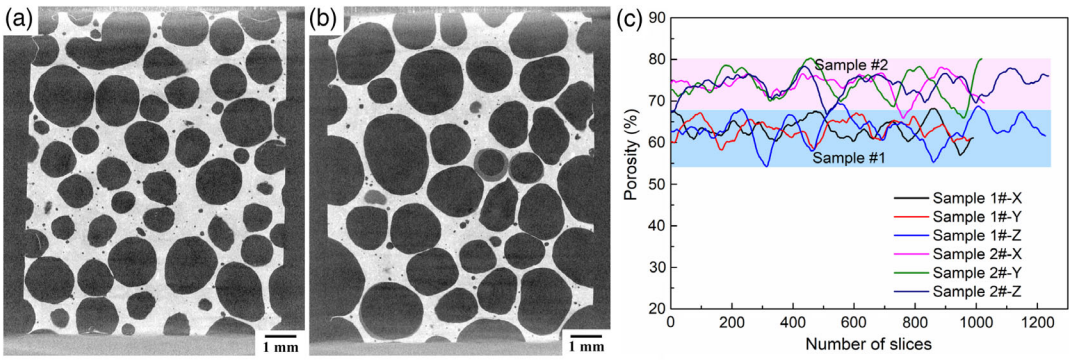

Figure 1. A tomographic slice of a) sample #1 and b) sample #2, and c) porosity distributions of tomography slices of the two samples along the three directions.

according to Figure 1c, so the size effect could be further reduced, and dimensions of the samples are considered enough.[46]

2.2. Quasi-Static Compression

A compressive device, which allows for X-ray tomography, was used for studying the evolution of cell structure during compression of aluminum foams. The compression rig was developed by MATEIS lab of Institut National des Sciences Appliquées de Lyon (INSA-Lyon). The foam sample was connected with a force sensor and placed into an aluminum tube of 1 mm wall thickness and 15 mm inner diameter. After the tube was connected with a motor, the whole assembled device was placed on the rotating stage in the X-ray equipment. The detailed description of the device is given in the literature.[14,23,47] The height of the sample in compressive direction was around 10 mm, and the strain rate was $5 \times 10^{-4}\ s^{-1}$, so the compression was in quasi-static condition. The compression motion stopped for X-ray tomography scanning each 0.3 mm (the first 12 tomograms) or 0.5 mm (the rest tomograms) loading. One sample was scanned around 20 times during the whole compressive process, and each tomogram took around half an hour. The resolution of the X-ray tomography was 8 µm voxel size. The load–displacement curve could be obtained after compression, from which the corresponding stress–strain curve was calculated.

2.3. Research Methods

The samples were first cropped to leave only the volume with internal cells and cell walls. Then, after the processes of binarization, watershed, border kill, etc., the cell size, anisotropy, sphericity, orientation, and spatial coordinates of each cell in different conditions could be obtained by the software Avizo. Thicknesses of solid part, including cell membranes and plateau borders, were obtained by the plugin "local thickness" in the software Fiji. Porosity distribution of tomography slices was also calculated in software Fiji. The coordination number was calculated by the spatial coordinates using the software Matlab. The correlation between the deformation degree and initial cell parameters was fitted from one sample and then verified by the result from the other sample. Using obtained theoretical formula and initial cell parameters, locations of cells deformed in the first batch were predicted with Matlab and shown with Avizo.

3. Results

3.1. Compressive Performance of the Two Samples

Figure 2a,b shows the stress–strain ($\sigma(\varepsilon)$–ε) curves of the two samples, which can be divided as elastic stage, stress plateau stage, and densification stage. Energy absorption efficiency $\eta(\varepsilon)$–ε curve is also plotted as a red dotted line in Figure 2a,b. **Table 1** shows the compressive performance of the two samples, and calculation formula of $\eta(\varepsilon)$, W_D and σ_P can be found in Equation S(1)–S(3), Supporting Information. It could be observed that the plateau stress and energy absorption of sample #1 are both higher than #2 because of the higher relative density.[3] The higher ε_0 indicates that sample #1 enters the plateau stage later than sample #2. The elastic modulus in the elastic stage of sample #2 is higher than that of #1, which is caused by the difference of cell structure, and will be discussed in Section 4.3. Figure 2c,d shows the porosity distribution of tomography slices along the height of the two samples under different strains. The local high porosity region is continuous as the strain increases, which means the local low-density region was not the main deformation area during the early compressive process, and the difference of deformation along the axis is not obvious. The influence of an individual cell structure should be considered for these low porosity aluminum foams (<75%).

3.2. Initial Cell Parameters of the Two Aluminum Foam Samples

Based on the listed cell parameters, which affect the deformation in Section 1 and the analysis in Section 3.1, the initial cell parameters of the two samples before deformation were analyzed in detail. 1) Equivalent cell diameter (d_e): The equivalent cell diameter distribution of the two samples in the undeformed condition is shown in Figure S1, Supporting Information. There are many micropores in both foams in Figure S1, Supporting Information,

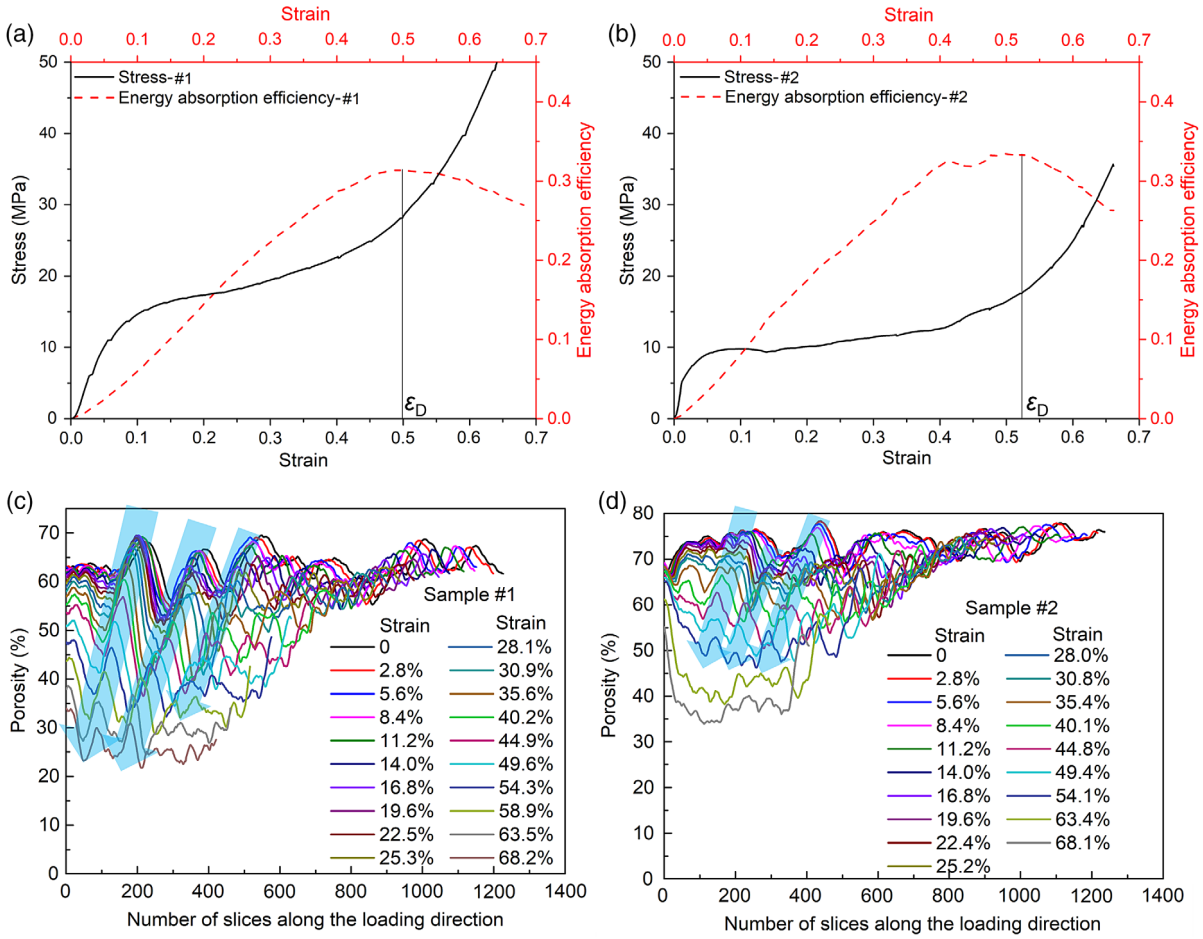

Figure 2. The stress–strain curve of a) sample #1 and b) sample #2, and porosity distribution of tomography slices along the height under different strains for c) sample #1 and d) sample #2.

Table 1. Compressive performance of the two aluminum foam samples.

Parameters	Sample #1	Sample #2
Porosity [%]	62.0	73.3
First peak stress, σ_0 [MPa]	16.2	9.8
Strain at the first peak stress, ε_0	0.138	0.097
Plateau stress, σ_P [MPa]	20.6	12.0
Densification strain, ε_D	0.499	0.523
Densification strain energy, W_D [MJ m^{-3}]	8.90	5.89

Table 2. Statistical initial cell parameters of the two aluminum foam samples.

Initial cell parameters	Sample #1		Sample #2	
	Average value	Standard deviation	Average value	Standard deviation
Equivalent cell diameter [mm]	1.32	0.34	1.63	0.48
Solid material thickness [mm]	0.246	0.081	0.223	0.080
Sphericity	0.893	0.044	0.909	0.028
Anisotropy	0.360	0.155	0.396	0.114
Angle between the longest axis of a cell and loading direction [°]	56.2	20.5	62.3	16.2
Coordination number	7.0	3.3	5.6	3.4

which can also be observed in Figure 1. The tremendous amount of micropores are mostly formed by entrapped gas from the blowing agent or present in the melt, or during solidification, which are not considered to study the evolution of the macroscopic cell structure of the foam. Referencing to the Gauss cell size distribution, cells with a diameter of less than 0.7 mm were not considered during calculation. The incomplete cells on the boundary were also dismissed during analysis to avoid edge effects. The average value and standard deviation of cell diameter in the two samples are listed in **Table 2**. 2) Thickness of solid part (t): Local thickness of a point in the cell membranes or plateau borders is the diameter of the largest sphere that contains the point and fits inside the local

solid, which is computed in terms of a distance ridge after producing a distance map with Fiji.[48] One slice of the calculation for each sample is shown in Figure S2a,b, Supporting Information, where different 3D solid thicknesses are represented by different colors. The distribution of the solid thickness is shown in Figure S2c,d, Supporting Information. The statistical results are listed in Table 2. 3) Sphericity (Ψ): Sphericity is the inverse ratio of the surface area of a cell and of a sphere, which has the same volume as the cell itself. The sphericity is 1 for an ideal spherical cell. Sphericity reflects how closely the shape of a cell approaches to a perfect sphere in terms of surface area. Figure S3a,b, Supporting Information, shows the cell sphericity distribution of the two samples, and the statistical results are listed in Table 2. The sphericity of most cells in both foams is relatively high and concentrated between 0.85 and 0.95. 4) Anisotropy (A): Anisotropy is 1 minus the ratio of the smallest to the largest eigenvalue of the covariance matrix of the cellular structure, which could measure an object's deviation from a sphere. Compared with sphericity, anisotropy emphasizes the chord length difference of a cell in different directions. According to the definition of anisotropy in this article, the anisotropy of an ideal spherical cell is 0. The cell anisotropy distribution of the two samples is shown in Figure S3c,d, Supporting Information, and the statistical results are listed in Table 2. It can be seen that the distribution of cell anisotropy in both foams is quite scattered. 5) Cell orientation: To characterize the orientation of a cell, the parameter "EigenVec1Z" was used. EigenVec1Z is the z coordinate of normalized eigenvector 1, which corresponds to the largest eigenvalue of the covariance matrix of a cell. Therefore, EigenVec1Z is the cosine of the angle (α) between the longest axis of a cell and the loading direction. Considering that the contributions of positive and negative values of EigenVec1Z to compression performance are the same, the absolute value was used to calculate the angle α, namely, $\cos\ \alpha = |\text{EigenVec1Z}|$. Figure S3e,f, Supporting Information, shows the distribution of angle α of cells in both foams, and the statistical results are listed in Table 2. 6) Coordination number (n_c): The number of surrounding cells or neighbors of a cell is called the coordination number. If the spatial distance between the volume centers of two cells is not larger than the sum of their equivalent radius and a given solid material thickness, the two cells are defined as neighbors of each other. The solid material thickness was defined here as twice the average solid material thickness. The influences of cell wall thickness, cell size, and local density around a cell on cell deformation could also be indirectly reflected by coordination number. The distribution of the cell coordination number in both samples is shown in Figure S3g,h, Supporting Information, and the statistical results are listed in Table 2. The average coordination numbers of both foams are less than the one in other foam structures.[40] One reason is the low porosity of the two samples. The other is high proportion of cells on the boundary caused by the small sample size.

4. Discussion

4.1. Quantifying Cell Deformation by Image Analysis

4.1.1. Evaluation of the Cell Deformation Degree

Because the porosity of the samples is low, most cells of the sample have already a certain degree of deformation when the first batch of cells deforms relatively severely. **Figure 3** shows some selected, deformed cells from sample #1 at strain 0 and strain 17%, and the original equivalent diameter (d_e) of each cell is also indicated as a reference scale in the 3D image. An evaluation needs to be selected for quantitatively characterizing the cell deformation. It could be seen that cell parameters, which mainly change during compression, are cell size (or cell volume), sphericity, anisotropy, and cell orientation. Change of EigenVec1Z (related to cell orientation) is difficult to characterize, because the longest axis of a cell itself may change abruptly during compression (as shown in Figure 3e), and then, the angle with loading direction will also change abruptly. Therefore, change degrees of volume, equivalent diameter, sphericity, and anisotropy of every cell could be used to evaluate the deformation of cells.

Cells of sample #1 at the strain of 11% and 17% were tracked and compared with the initial undeformed cells separately. The first and second columns in **Figure 4**a show the change degrees of volume of every cell when the strain of sample #1 changes from 0% to 11% (V-11) and from 0% to 17% (V-17). Similarly, change degrees of equivalent diameter (D-11 and D-17), sphericity (S-11 and S-17), and anisotropy (A-11 and A-17) in the two situations are also presented accordingly. Change degrees of volume (V-11), diameter (D-11), sphericity (S-11), and anisotropy (A-11) when the strain varies from 0% to 11% in sample #2 are shown in Figure 4b. The positive degree of change of every parameter is defined as follows: cell volume and cell equivalent diameter become smaller, cell sphericity becomes smaller, and cell anisotropy becomes larger. Figure 4a,b indicates that the change degree of cell anisotropy is the largest. Therefore, anisotropy as the most sensitive parameter during compression is selected in this work to evaluate the cell deformation.

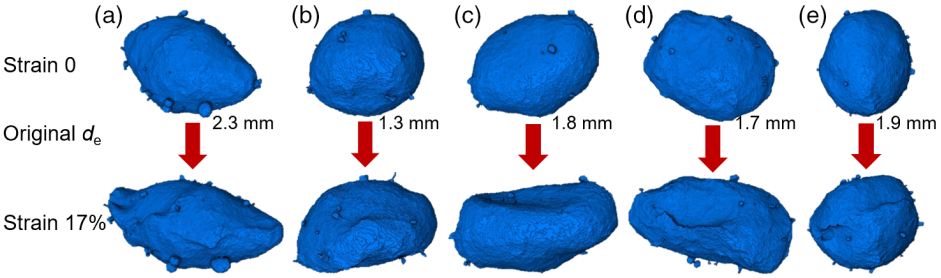

Figure 3. a–e) Five deformed cells from sample #1 at strain 0 and strain 17%, and all views are in the *xz* plane.

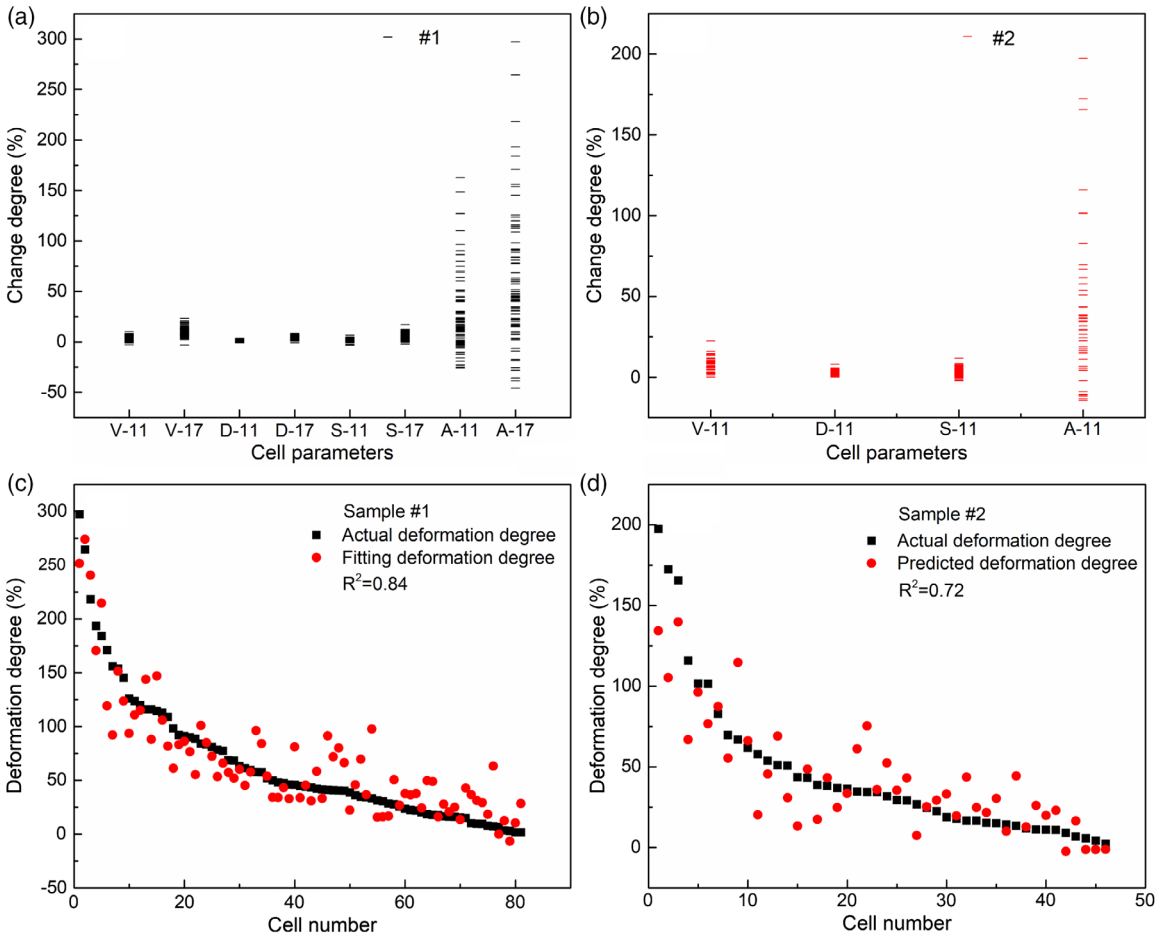

Figure 4. Change degrees of different cell parameters at the strain of a) 11% and 17% for sample #1 and b) 11% for sample #2, c) comparison of actual and fitted deformation degree of every cell in sample #1 at strain 17%, and d) comparison of actual and predicted deformation degree of every cell in sample #2 at strain 11%.

In Figure 4a, the distribution range at the strain of 17%, under the description of all cell parameters, is larger than that at 11%. Combined with the stress–strain curve in Figure 2a, 17% also represents the strain just after the first peak stress of sample #1. Most cells start to plastically deform, and some cells deform severely as the first batch, but are still recognizable at this state, which is suitable to study the effects of initial cell factors on cell deformation. Therefore, the cell structure at the strain of 17% was taken to study the cell deformation of sample #1. Similarly, combined with Figure 2b, the strain of 11% was selected for sample #2 after analysis.

4.1.2. The Correlation between the Deformation Degree and Initial Cell Parameters

Considering that the cell deformation is always positive, the absolute value of anisotropy change was defined as the cell deformation degree. Initial cell parameters of every cell of sample #1 in Section 3.2 were used to fit the cell deformation degree at strain 17%. After fitting optimization, the obtained regression formula is Equation (1).

$$P = 565 - 2028A - 18|e_z| - 185\psi + 3n_c + 5d_e + 3483A^2 - 2025A^3 \quad (1)$$

where P is the deformation degree of a cell given in percentage. e_z is EigenVec1Z, namely, the z coordinate of normalized eigenvector 1; also, the absolute value was used in the fitting. Unit of the cell equivalent diameter (d_e) is mm.

The goodness of fit (R^2) is 0.84 in the regression. Figure 4c shows the comparison of the actual and fitted deformation degrees of every cell in sample #1 at strain 17%. The abscissa is the cell number of sample #1, which is arranged in the descending order of actual anisotropy. It can also be observed that the fitting and actual results agree well.

To verify the regression formula, Equation (1) was used to calculate and predict the cell deformation degree in sample #2. Then, the results were compared with the actual cell deformation degree of sample #2 at strain 11%, which is also the strain where the first batch of cells deformed. Figure 4d shows the comparison results, and the cell number is also arranged in the descending order of actual anisotropy. The deviation between the actual and predicted results is a bit large when the actual deformation

degree is high, which should be caused by two reasons: 1) The three cells with the highest actual deformation degree are all located at the boundary or corner of sample #2, so the error of the calculated coordination numbers may influence the result. 2) Strain 11% for sample #2 was chosen for study, because it was just after the peak stress and the first batch of cells have deformed. It was difficult to find a strain for sample #2 exactly the same state as sample #1 at strain 17%, and this could cause the error. However, the deformation degree of most cells in sample #2 could be predicted well by Equation (1), and the goodness of fit is 0.72.

According to Equation (1), contribution of each cell parameter to cell deformation could be studied. The cell characteristics that tend to trigger cell deformation are as follows: 1) Small anisotropy: By extracting the three items related to anisotropy in Equation (1), as shown in Figure S4a, Supporting Information, it could be found that the anisotropy is negatively correlated with cell deformation degree, so a cell with small anisotropy is easier to deform. The influence of anisotropy is also consistent with the study from other researchers.[5,40] 2) Small absolute value of EigneVec1Z: i.e., the angle between the longest axis of the cell and Z axis is large. 3) Small sphericity: The cell with large surface area under the same volume is prone to deform. 4) Large coordination number: A cell with more neighbors has a higher tendency to deform. 5) Large cell size: A large cell is prone to deform compared with a small one. Usually, a cell with large cell size has large coordination number, so the effects of these two factors are consistent.

4.2. Prediction of the First Deformed Cells in Aluminum Foams

The deformation degree of each cell can be obtained by the initial cell parameters of the foam with Equation (1). Then, if the calculated deformation degrees are associated with the initial 3D image data of the foam, the first severely deformed cells can be determined. **Figure 5** shows the prediction result of cells that are more prone to deform in a 3D rendered tomogram for samples #1 and #2. It could be seen that more cells in the upper region of sample #1 have a high deformation degree; therefore, the first deformed cells are more probable to appear in this part. Accordingly, the first batch of cell failures is more likely to appear in the middle and lower regions for sample #2. However, the failure layer by layer as a crash band as reported in the literature[49] is not obvious in both samples due to high relative densities. The prediction of the first deformed cells is very meaningful for applications. The weakest region inside the foam based on the initial 3D foam structure could be predicted in advance, and together with a selection criterion used as a non-destructive quality control.

4.3. Influence of Cell Morphology on Deformation of Low Porosity Aluminum Foams

Compared with the foam deformation analysis based on cell walls of high porosity aluminum foams in previous research,[21,29,32] our work demonstrates that the cell morphology plays an important role for the first deformation of aluminum foams with low porosity (<75%) and relatively uniform cells. Influences of cell morphology parameters on cell deformation were quantitatively characterized. According to the regression

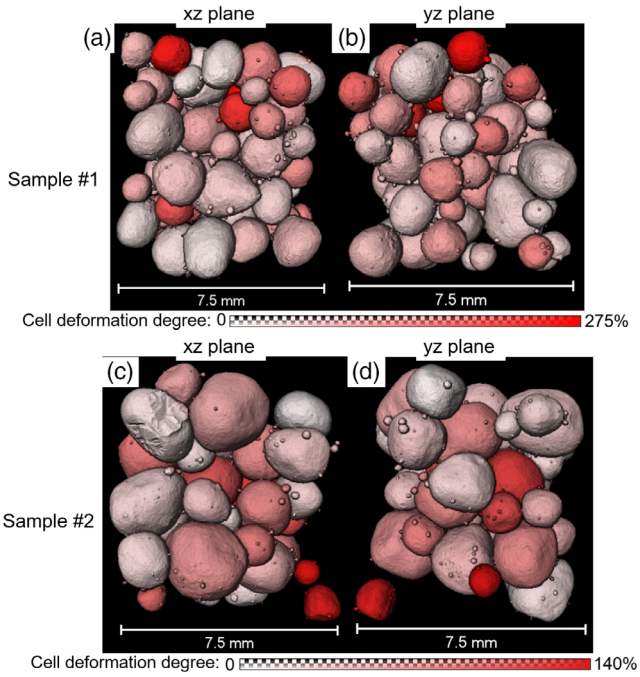

Figure 5. Prediction of cells that more prone to deform in a,b) sample #1 and c,d) #2. a,c) Views from the *xz* plane. b,d) Views from the *yz* plane.

formula of Equation (1), contributions of different cell parameters in a certain range to the cell deformation degree are described in Figure S4, Supporting Information. It could be seen that effects of cell shape parameters anisotropy and sphericity are more significant than other factors. That is why the elastic modulus of sample #2 is larger than that of #1 in the elastic stage, as shown in Figure 2a,b. The cells with larger anisotropy and sphericity in sample #2 are more difficult to deform, and the sample can withstand higher stress in the first stage. After the first batch of cells is deformed, the lower relative density of sample #2 causes the lower plateau stress.

Figure 6 shows the sphericity and anisotropy distributions of the two samples in different compressive strains. Considering cells get smaller under large strains, 0.35 mm was taken as the criteria of removing micropores during the statistics of Figure 6. At strain 17% for sample #1 and 11% for sample #2, the peak sphericity in the distribution both decreased a lot, and the peak anisotropy both increased obviously. This indicates the first batch of cells for the two samples deformed severely at these two strains, respectively. Cells with small anisotropy are easier to deform, as shown in Figure 6c,d. Although the overall decreasing of cell sphericity during compression caused the changing of peak value in Figure 6a,b, the insets show cells with smaller sphericity deform earlier. Therefore, cells with small anisotropy and small sphericity are easier to deform, which agree with the prediction of the formula.

5. Conclusion

1) The detailed cell structure information of the studied aluminum foams at different stages of compression was obtained by a compressive test with complementary X-ray tomography. 2) The

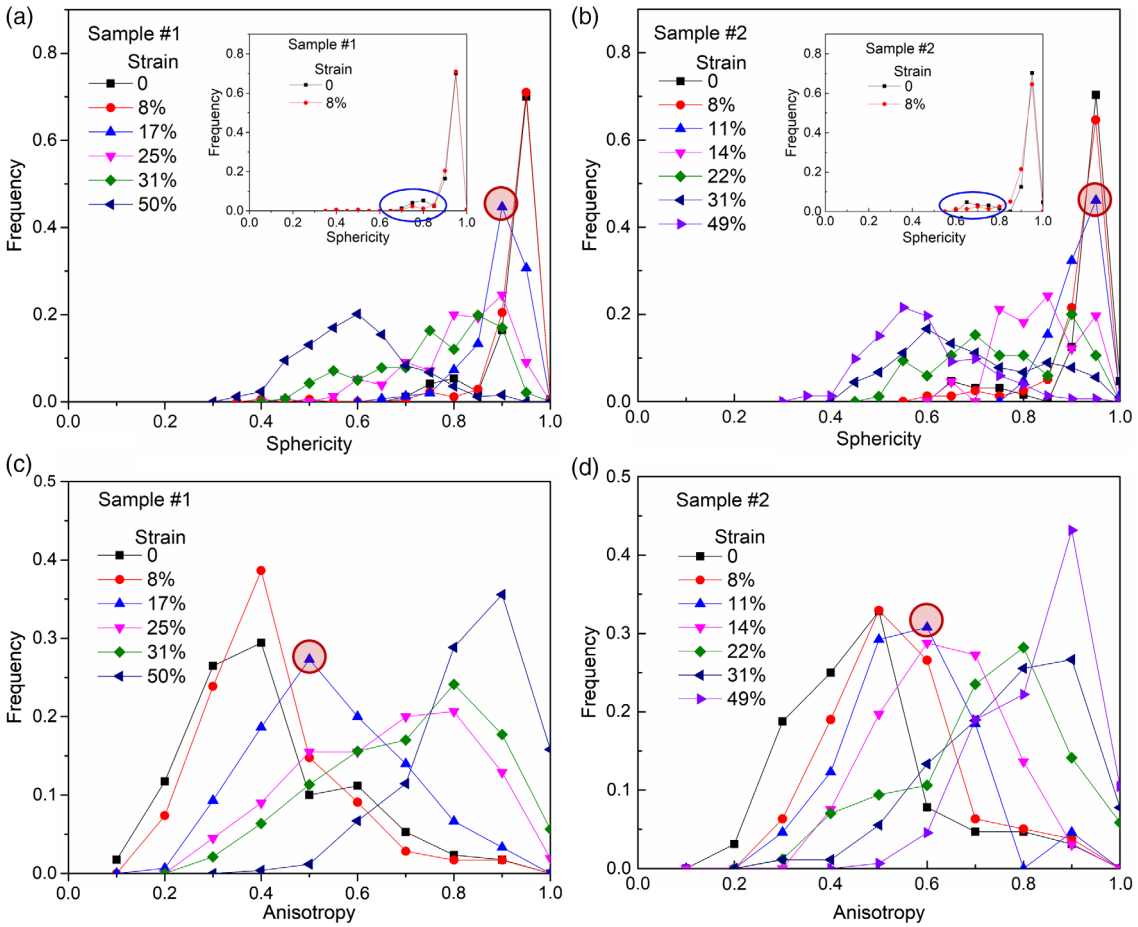

Figure 6. Sphericity distribution of a) sample #1 and b) #2 in different strains (the insets contain the results under the first two strains), and anisotropy distribution of c) sample #1 and d) #2 in different strains.

cell parameters at the first batch of deformed cells were characterized, which helps to study the cell characteristics that trigger cell deformation. Cell size (or cell volume), sphericity, anisotropy, and cell orientation all changed during deformation, but the cell anisotropy was found to be the most sensitive parameter. Therefore, the absolute value of anisotropy change was used to evaluate the cell deformation. 3) A regression formula between the cell deformation degree and the initial cell parameters was obtained, which could predict the cell deformation degree when the first batch of cells deforms. It has been found that a cell with small anisotropy, large angle between the longest axis of the cell and the loading direction, small sphericity, more neighbors, and large cell size is more prone to deform during compression. 4) With the fitting formula, the weakest region with the first batch of deformed cells could be predicted based on the initial 3D foam structure. This is a quite meaningful tool for applications. For the low porosity aluminum foams, the cell morphology parameters play an important role in the deformation of the first batch of cells.

Supporting Information

Supporting Information is available from the Wiley Online Library or from the author.

Acknowledgements

The authors thank the Deutsche Forschungsgemeinschaft for the support, grant GA 1304/5-1, AOBJ 622125. The authors also would like to thank Dr. Guoyu Guan from Northeast Normal University for the discussion of regression formula.

Conflict of Interest

The authors declare no conflict of interest.

Keywords

aluminum foam, cell deformation prediction, cell structure, X-ray tomography

Received: March 5, 2020
Revised: May 12, 2020
Published online: June 3, 2020

[1] J. Banhart, *Prog. Mater. Sci.* **2001**, *46*, 559.
[2] F. García-Moreno, *Materials* **2016**, *9*, 85.

[3] L. J. Gibson, M. F. Ashby, *Cellular Solids: Structure and Properties*, Cambridge University Press, Cambridge **1997**.
[4] D. Wang, W. Xue, X. Meng, Z. Shi, *J. Mater. Sci.* **2005**, *40*, 3475.
[5] J. Kadkhodapour, S. Raeisi, *Comp. Mater. Sci.* **2014**, *83*, 137.
[6] X. Chen, N. Wang, J. Yuan, Y. Li, H. Zhang, Y. Liu, *J. Mater. Eng. Perform.* **2017**, *26*, 3307.
[7] T. Shi, X. Chen, Y. Cheng, Y. Liu, H. Zhang, Y. Li, *Mater. Trans.* **2018**, *59*, 625.
[8] E. Maire, *Annu. Rev. Mater. Res.* **2012**, *42*, 163.
[9] N. Wang, E. Maire, Y. Cheng, Y. Amani, Y. Li, J. Adrien, X. Chen, *Mater. Charact.* **2018**, *138*, 296.
[10] Y. P. Jeon, C. G. Kang, S. M. Lee, *J. Mater. Process. Tech.* **2009**, *209*, 435.
[11] Y. Zou, D. He, J. Jiang, *Sci. China Ser. B* **2004**, *47*, 407.
[12] J. Lázaro, E. Solórzano, M. A. Rodríguez-Pérez, *Adv. Eng. Mater.* **2017**, *19*, 1600496.
[13] Y. Hangai, R. Yamaguchi, S. Takahashi, T. Utsunomiya, O. Kuwazuru, N. Yoshikawa, *Metall. Mater. Trans. A* **2013**, *44*, 1880.
[14] N. Wang, E. Maire, X. Chen, J. Adrien, Y. Li, Y. Amani, L. Hu, Y. Cheng, *Mater. Charact.* **2019**, *147*, 11.
[15] H. Zhang, X. Chen, X. Fan, Y. Li, *China Foundry* **2012**, *9*, 215.
[16] A. T. Barnes, K. Ravi-Chandar, S. Kyriakides, S. Gaitanaros, *Int. J. Solids Struct.* **2014**, *51*, 1631.
[17] L. Wang, Y. Ding, L. Yang, *Int. J. Impact Eng.* **2013**, *62*, 48.
[18] Y. Sun, X. Zhang, Z. Shao, Q. M. Li, *Mater. Sci. Eng., A* **2017**, *688*, 27.
[19] B. M. Patterson, K. Henderson, Z. Smith, *J. Mater. Sci.* **2013**, *48*, 1986.
[20] M. A. Kader, A. D. Brown, P. J. Hazell, V. Robins, J. P. Escobedo, M. Saadatfar, *Int. J. Impact Eng.* **2020**, *139*, 103510.
[21] H. W. Chai, H. Y. Li, X. H. Xiao, J. Y. Huang, S. N. Luo, *Scr. Mater.* **2019**, *170*, 177.
[22] H. W. Chai, Z. L. Xie, X. H. Xiao, H. L. Xie, J. Y. Huang, S. N. Luo, *Int. J. Plasticity* **2020**, 102730, https://doi.org/10.1016/j.ijplas.2020.102730.
[23] C. Petit, E. Maire, S. Meille, J. Adrien, *Mater. Design* **2017**, *120*, 117.
[24] B. Pan, B. Wang, *Meas. Sci. Technol.* **2017**, *28*, 105007.
[25] O. Jiroušek, T. Doktor, D. Kytýř, P. Zlámal, T. Fíla, P. Koudelka, I. Jandejsek, D. Vavřík. *J. Instrum.* **2013**, *8*, C02012.
[26] R. Edwin Raj, V. Parameswaran, B. S. S. Daniel, *Mater. Sci. Eng., A* **2009**, *526*, 11.
[27] A. E. Simone, L. J. Gibson, *Acta Metall.* **1998**, *46*, 2139.
[28] A. E. Simone, L. J. Gibson, *Acta Metall.* **1998**, *46*, 3929.
[29] Y. Mu, G. Yao, L. Liang, H. Luo, G. Zu, *Scr. Mater.* **2010**, *63*, 629.
[30] H. Song, Q. He, J. Xie, A. Tobota, *Compos. Sci. Technol.* **2008**, *68*, 2441.
[31] A. Bastawros, H. Bart-Smith, A. G. Evans, *J. Mech. Phys. Solids* **2000**, *48*, 301.
[32] M. A. Kader, M. A. Islam, M. Saadatfar, P. J. Hazell, A. D. Brown, S. Ahmed, J. P. Escobedo, *Mater. Design* **2017**, *118*, 11.
[33] Z. Cao, M. Li, Y. Yu, H. Luo, *Adv. Eng. Mater.* **2016**, *18*, 1022.
[34] Y. Cheng, Y. Li, X. Chen, T. Shi, Z. Liu, N. Wang, *Metall. Mater. Trans. B* **2017**, *48*, 754.
[35] X. Zhou, Y. Li, X. Chen, *J. Mater. Process. Tech.* **2020**, *283*, 116698.
[36] T. Miyoshi, M. Itoh, S. Akiyama, A. Kitahara, *Adv. Eng. Mater.* **2000**, *2*, 179.
[37] Y. Cheng, Y. Li, X. Chen, X. Zhou, N. Wang, *J. Mater. Eng. Perform.* **2018**, *27*, 4016.
[38] S. A. Meguid, S. S. Cheon, N. El-Abbasi, *Finite Elem. Anal. Des.* **2002**, *38*, 631.
[39] Y. Hangai, K. Takahashi, R. Yamaguchi, T. Utsunomiya, S. Kitahara, O. Kuwazuru, N. Yoshikawa, *Mater. Sci. Eng., A* **2012**, *556*, 678.
[40] M. Saadatfar, M. Mukherjee, M. Madadi, G. E. Schröder-Turk, F. Garcia-Moreno, F. M. Schaller, S. Hutzler, A. P. Sheppard, J. Banhart, U. Ramamurty, *Acta Mater.* **2012**, *60*, 3604.
[41] X. Yang, W. Wang, L. Yan, Q. Zhang, T. J. Lu, *J. Phys. D Appl. Phys.* **2016**, *49*, 505301.
[42] W. Jang, W. Hsieh, C. Miao, Y. Yen, *Mater. Charact.* **2015**, *107*, 228.
[43] Z. Liu, Y. Cheng, Y. Li, X. Zhou, X. Chen, N. Wang, *Int. J. Miner. Metall. Mater.* **2018**, *25*, 974.
[44] E. W. Andrews, G. Gioux, P. Onck, L. J. Gibson, *Int. J. Mech. Sci.* **2001**, *43*, 701.
[45] Y. Zhang, T. Jin, S. Li, D. Ruan, Z. Wang, G. Lu, *Int. J. Mech. Sci.* **2019**, *151*, 622.
[46] I. Jeon, T. Asahina, *Acta Mater.* **2005**, *53*, 3415.
[47] J. Y. Buffiere, E. Maire, J. Adrien, J. P. Masse, E. Boller, *Exp. Mech.* **2010**, *50*, 289.
[48] R. P. Dougherty, K. H. Kunzelmann, *Microsc. Microanal.* **2007**, *13*, 1678.
[49] M. Mukherjee, M. Kolluri, F. Garcia-Moreno, J. Banhart, U. Ramamurty, *Scr. Mater.* **2009**, *61*, 752.